Applied Catalysis A, General 577 (2019) 28–34

Contents lists available at ScienceDirect

Applied Catalysis A, General

journal homepage: www.elsevier.com/locate/apcata

Synthesis and catalytic testing of Lewis acidic nano zeolite Beta for epoxide ring opening with alcohols

Aamena Parulkar, Alexander P. Spanos, Nitish Deshpande, Nicholas A. Brunelli*

Ohio State University, William G. Lowrie Department of Chemical and Biomolecular Engineering, 151 W. Woodruff Ave., Columbus, OH 43210, United States

ARTICLE INFO

Keywords:
Alcohol ring opening of epoxides
Nano zeolites
Lewis acidic zeolites
Pore-limited diffusion

ABSTRACT

Lewis acidic zeolites are robust catalytic materials that are capable of a range of important chemistry for fine chemical production, including the epoxide ring opening with alcohols. The crystalline structure imposes diffusion limitations for large molecules that are overcome through reducing the particle size to produce nano zeolite beta substituted with Lewis acidic tin (nSnBeta). nSnBeta is characterized using standard methods to demonstrate that tin is efficiently incorporated into the zeolite framework with open and closed sites similar to the micron-sized conventional Sn-Beta (cSnBeta). While nSnBeta exhibits comparable catalytic activity to cSnBeta for reactions involving small substrates such as epichlorohydrin and methanol, an improvement in catalytic performance is observed for nSnBeta relative to cSnBeta when using large substrates such as 1,2-epoxyoctane and ethanol. nSnBeta and cSnBeta convert a cyclic epoxide too large to enter the pores to similar extents, indicating that the improved performance is not associated with an increased number of catalytic sites on the external surface. Catalyst reuse experiments demonstrate that organic accumulation on the material reduces catalytic activity that can be partially restored through calcination. Overall, the results demonstrate that nano zeolite beta can be synthesized with small particle sizes (*i.e.*, 150 nm) to help overcome diffusion limitations for bulky substrates for the alcohol ring opening of epoxides.

1. Introduction

Advances in catalysis using Lewis acidic materials are transforming the ability to produce chemicals in a sustainable manner. Indeed, Lewis acidic zeolite catalysts containing heteroatoms such as tin (Sn), titanium, zirconium, and hafnium in different zeolites frameworks [1–4] have been shown to catalyze a variety of industrially important chemical reactions such as biomass upgrading [5–7], Meerwein-Ponndorf-Verley (MPV) [8,9], Baeyer-Villiger (BV) oxidation [10,11], Diels-Alder chemistry [12], aldol condensation [13,14], epoxidation [4,15], and ring-opening of epoxides [16,17]. This impressive array of chemistry can have limited reaction scope because of the small pores associated with zeolites that can introduce significant internal mass transfer limitations. Therefore, it is an important challenge to design catalytic materials to overcome these limitations to further expand the scope of available chemical reactions.

Current research is investigating methods to overcome internal mass transfer limitations through controlling material synthesis. The primary goal has been to reduce the internal diffusion path length through either creating hierarchical zeolites or nano zeolites [18–23]. Hierarchical zeolites provide a simple and efficient way to mitigate diffusion limitations within zeolites at the expense of the structural stability of these materials. In certain cases, the presence of mesopores can also affect the shape selectivity and therefore precise design of catalysts is required [24]. An interesting alternative is to reduce the particle size. With the synthesis of MFI nano-sheets, it has been demonstrated that nano zeolites can significantly improve the catalytic performance [25,26].

As the catalytic behavior for zeolite catalysts is strongly dependent on the type of framework, the pore size and network can influence the selectivity of a chemical reaction. Even with the nanoscale dimensions, MFI nanomaterials have limited catalytic activity for certain reactions, given the small pore size (10 membered ring, 10MR). While MFI has a 10MR pore architecture, zeolite beta has a 12MR in the framework, providing a catalyst structure that can be employed for larger substrates. Therefore, developing methodologies to reduce particle size for zeolite beta is of importance, especially with Lewis acidic heteroatom incorporation.

The synthesis procedure can be modified to tune the particle size for zeolite Beta. While zeolite crystallization is a complex phenomenon and not yet completely understood, studies have sought to understand the effect of different synthesis parameters on the crystallization [27–29].

---

* Corresponding author.
E-mail address: brunelli.2@osu.edu (N.A. Brunelli).

https://doi.org/10.1016/j.apcata.2019.03.009
Received 30 December 2018; Received in revised form 11 March 2019; Accepted 17 March 2019

To reduce particle size for zeolite Beta, several methods have been investigated, including the addition of seeds, confined space synthesis, novel structure directing agents (SDAs), and dry-gel interconversion [21,30–35]. While these studies demonstrate the benefits of nanosized zeolite, they are focused on either purely siliceous or aluminosilicate zeolite beta. Translating this work for synthesizing Lewis acidic zeolites can be challenging since incorporating heteroatoms like Sn, Zr, and Hf can significantly influence zeolite crystallization. Indeed, Sn inclusion is known to slow the crystallization of zeolite beta, especially at high Sn concentration [36]. The slow crystallization results in larger particle size as well as increased intergrowth. These micron-sized particles of Sn-beta can pose diffusion limitations when utilizing bulky substrates [37].

Recent studies have demonstrated synthesis of nano-sized Sn-Beta through both hydrothermal and post-synthetic routes [22,38,39]. Post-synthetic routes to nano-Sn-Beta utilized either partially crystalline Si-beta or dealuminated beta as the starting material. While post-synthetic routes can be efficient, these methods tend to produce materials that are less active than hydrothermally crystallized zeolites [40]. It has also been demonstrated that nano Sn-Beta can be produced through hydrothermal methods using *N*-cyclohexyl-*N*,*N*-dimethyl cyclohexanaminium hydroxide as the SDA [39]. This SDA could be used under hydroxide-mediated conditions and resulted in a particle size of Sn-Beta of ∼500 nm. Overall, these methods reduced the particle size below a micron, but the particles are still larger than 200 nm. Recent work with nano-Sn-MFI demonstrated the diffusion limitations for the epoxide ring–opening reaction with 1,2-epoxyhexane and methanol were not substantially reduced until the particle size is reduced below 200 nm [17]. Therefore, it is important to investigate additional synthetic methods that can achieve catalytic particles with a size smaller than 200 nm.

An SDA that has been demonstrated for successful synthesis of zeolite Beta with ∼140 nm particle size is 4,4′-trimethylenebis(N-methyl, N-benzyl piperidinium) cations (TMP) [21]. However, this SDA has only been utilized for purely siliceous or aluminum containing zeolite Beta. The observed reduction in particle size while utilizing TMP as the SDA can be partly attributed to the basic conditions of the synthesis gel [41]. Therefore, this makes TMP a possible SDA for examining synthesis of Lewis acidic nano Beta zeolite.

Lewis acidic zeolites, both post-synthetically and hydrothermally synthesized, including Sn-H-SSZ-13, Sn-Beta, Zr-Beta, and Hf-Beta, have been shown to catalyze ring-opening of epoxides using amines, water, and alcohols as the nucleophiles [16,42–44]. Specifically, ring-opening of epoxides with alcohols results in formation of β-alkoxy alcohols, which find application as intermediates in pharmaceutical and solvent industry [45]. The activity for ring-opening of epoxides with alcohols can be enhanced by using Lewis acidic zeolites [43]. However, the small pores associated with the zeolite framework may introduce diffusion limitations that necessitate utilization of nano zeolites to enable conversion of a broad scope of substrates.

In this work, the synthesis of nano zeolite Beta substituted with tin (nSnBeta) is examined using hydrothermal conditions with TMP cations as the SDA to produce particles less than 200 nm. The incorporation of Sn at Si to Sn ratio of 100 and 200 is investigated and compared to traditional hydrothermal synthesis of Sn-Beta. The materials are characterized using a battery of standard techniques to investigate particle size, tin incorporation efficiency, and the nature of the Sn species. The nSnBeta catalysts are tested and compared to conventional SnBeta (cSnBeta) and nanoSnMFI (nSnMFI) catalysts for epoxide ring opening reaction of 1,2-epoxyoctane with ethanol. The stability and reusability of the catalyst is tested by performing recycling experiments. Overall, the work demonstrates the synthesis of nSnBeta and the catalytic capabilities of these materials to overcome diffusion limitations.

2. Experimental methods

2.1. Synthesis procedure for nSiBeta and nSnBeta

The pure silica form of zeolite beta with nanoscale dimensions (nSiBeta) is synthesized using the procedure previously reported in literature [21]. Briefly, the SDA is synthesized as detailed in the supplementary information (SI) according to previous methods [21]. Tetraethyl orthosilicate (TEOS; 5.02 g) is added to a round-bottom flask. In a separate flask, 18.06 g of 9.5 wt% $TMP(OH)_2$ hydroxide solution is weighed and then added to TEOS slowly with rapid stirring, maintaining the solution overnight at room temperature to ensure complete hydrolysis of TEOS. The mixture is evaporated under reduced pressure on a rotary evaporator with heating to 40 °C to remove excess water and ethanol. Three cycles of evaporation are performed with addition of 5 mL DI water in between each cycle. After the final cycle, the weight of synthesis gel is adjusted by adding DI water to achieve a gel composition of 1 SiO_2:0.15 TMP^{2+}:25 H_2O. The synthesis gel is transferred to a Teflon liner and 5 wt% of calcined Si-Beta seeds are added to facilitate crystallization. The Teflon liner is finally sealed inside an acid digestion vessel and placed in an oven preheated to 100 °C equipped with rotation at 35 RPM. The material is allowed to crystallize for 5 days after which the reactor is removed from the oven and quenched using tap water. The solids are separated by centrifugation at 9000 RPM for 10 min and the eluent is removed. The solids are then washed 5 times using 40 mL of DI water for each cycle. The washed solids are dried in an oven at 80 °C overnight followed by calcination at 550 °C (ramp rate of 2 °C/min) for 10 h in air using a Lindberg Blue M Moldatherm Box Furnace.

For synthesizing nano zeolite Beta with tin (nSnBeta), the synthesis procedure is modified to include $SnCl_4{\cdot}5H_2O$ as the tin source. While TEOS hydrolyzes in the presence of $TMP(OH)_2$, a separate solution of $SnCl_4{\cdot}5H_2O$ is prepared by dissolving the required amount of tin (depending on desired Si/Sn ratio) source in 1–2 mL of DI water. One hour after the initial mixing of $TMP(OH)_2$ and TEOS, the $SnCl_4$ solution is added to the mixture dropwise under vigorous stirring. The remaining steps of the procedure are similar to those for pure nSiBeta material. The final gel composition for nSnBeta materials is 1 SiO_2:x Sn:0.15 TMP^{2+}:25 H_2O, where x = 0.005 or 0.01 for a theoretical Si:Sn of 200:1 and 100:1. Similar synthesis with fluoride mediated conditions did not produce a crystalline product even after 90 days of crystallization time.

2.2. Synthesis procedure for conventional Sn-Beta

The synthesis is performed using the procedure reported previously [43]. Briefly, TEOS (24.48 g) is slowly added to 26.48 g TEAOH (35 wt % aqueous solution). The mixture is stirred for 90 min until a single-phase solution is formed. In a separate vial, the tin precursor solution is prepared by dissolving 0.206 g $SnCl_4{\cdot}5H_2O$ in 1.6 mL DI water. The Sn solution is added dropwise to the TEOS/TEAOH mixture. The mixture is allowed to hydrolyze overnight (20–24 h). The hydrolyzed mixture is concentrated using a rotovap three times to remove ethanol and some water, adding 20 g of DI water after each rotovapping cycle to remove the ethanol completely. DI water (1.28 g) is added to the final synthesis gel. The synthesis gel is then transferred to a Teflon-lined 200 mL acid-digestion vessel (Parr Inst. Comp.). Hydrofluoric acid (HF, 51 wt% aqueous solution; 2.0 mL) and 350 mg of calcined Si-Beta seeds are added to the synthesis gel and the mixture is stirred using a Teflon rod. The final gel composition is 1 SiO_2:0.005 Sn:0.54 F^-:0.54 TEA:7.5 H_2O. The acid digestion vessel is sealed and placed in a preheated oven at 140 °C with rotation at 35 RPM. The material is allowed to crystallize for 30 days. After the necessary crystallization time, the reactor is removed from the oven and quenched under tap water. The formed solids are filtered and washed with 1 L DI water. The filtered solids are dried in an oven at 80 °C overnight and then calcined in air at 550 °C for 10 h to remove the SDA.

2.3. Synthesis procedure for nanoSnMFI (nSnMFI-100)

Nano SnMFI (nSnMFI) is synthesized using a procedure described previously [17]. Briefly, 20.81 g of TEOS is mixed with 18.30 g of TPAOH and 29.77 g of DI water. In a separate vial, 0.5 g of $SnCl_4·5H_2O$ is mixed with 1.0 g of DI water. This solution is added to the TEOS/TPAOH mixture to give a molar ratio of the precursors of 1 TEOS: 0.02 Sn: 0.36 TPAOH: 23 H_2O. The synthesis gel is hydrolyzed for 24 h with stirring at room temperature and is then heated by submerging the flask in an oil bath, pre-heated to the 80 °C. The materials are allowed to crystallize for 20 days. The crystals are diluted with DI water and separated using centrifugation at 8500 rpm (Beckman Coulter Alegra X-30 centrifuge equipped with F0850 rotor model). After drying overnight, the materials are calcined at 560 °C for 3 h in air.

2.4. Material characterization

The materials are analyzed using a battery of standard characterization techniques, including nitrogen physisorption, powder X-ray diffraction (PXRD), scanning electron microscopy (SEM), diffuse reflectance infrared Fourier transform spectroscopy (DRIFTS), diffuse reflectance ultra-violet visible spectroscopy (DRUVS), thermogravimetric analysis-differential scanning calorimetry (TGA-DSC), and elemental analysis. The textural properties are characterized using a Micromeritics 3Flex surface characterization analyzer. The samples are first degassed on a Micromeritics SmartVacPrep sample preparation device at 140 °C under vacuum (10^{-3} mmHg) for 16 h followed by *in situ* degassing of samples on the 3Flex instrument for 4 h at 140 °C under vacuum (5×10^{-5} mmHg). The nitrogen sorption isotherms of degassed samples are recorded at liquid nitrogen temperatures (~77 K). The surface area and micropore volume of the materials are reported using BET and the t-plot method, respectively. The PXRD is collected using a Bruker powder X-ray diffractometer in flat plate reflection, Bragg Brentano optics mode using Cu $K_{\alpha 1}$–$K_{\alpha 2}$ radiation (λ = 1.540 and 1.544 Å) at 40 kV, 40 mA, and room temperature. The particle size and the morphology of the materials is analyzed using a FEI Nova 400 NanoSEM. SEM samples are prepared through dispersing the calcined material (~2 mg) in 100 μL methanol followed by deposition on conductive carbon tape. Prior to SEM analysis the samples are sputter-coated with ~8 nm thick layer of gold-palladium alloy using EMS 150 T S sputter coater. DRIFTS is performed using a Nicolet *iS*50 spectrometer equipped with MCT-A liquid nitrogen cooled detector (32 scans at 2 cm^{-1} resolution). The DRIFTS set up includes a Praying Mantis (Harrick Scientific Products, Inc.) with a high temperature reaction chamber consisting of zinc selenide (ZnSe) windows. The material is initially degassed *in situ* at 500 °C for 90 min under nitrogen flow before cooling to 25 °C. Similar to previous work [46], the material is pulsed with deuterated-acetonitrile using a VICI 6-port valve equipped with 100 μL sample loop. The probe molecule is allowed to desorb under nitrogen flow while increasing the temperature from 25 °C to 125 °C in steps, holding for 10 min at each temperature. The IR spectra are collected using a background of the degassed material at the same temperature before dosing. The DRUV–vis spectra are collected on Evolution 300 UV–vis spectrometer with a resolution of 2 nm at a rate of 10 nm s^{-1} with pure silica analogues of materials as the background. TGA is performed on a STA 449 F5 Jupiter® (NETZSCH instruments) under flowing air (20 mL min^{-1}) and nitrogen (20 mL min^{-1}; protective gas) at a ramp rate of 10 °C min^{-1} from 30 °C to 900 °C followed by a 5 min hold at 900 °C. Solution phase ^1H NMR spectroscopy of the synthesized SDA is performed using Bruker Advance III 400 MHz NMR spectrometer, using deuterated water as the solvent. All of the materials are characterized for elemental analysis by Galbraith Laboratories using inductively coupled plasma-optical emission spectroscopy (ICP-OES) to determine the weight percent of tin in the materials.

2.5. Catalytic testing

The catalytic testing is performed in a two neck 10 mL round bottom (RB) flask equipped with a condenser, a magnetic stir bar, and a septum. The RB is filled with 2 mL of a solution containing 0.4 M epoxide and diethylene glycol dibutyl ether (DGDE) as an internal standard in neat alcohol. A sample (40 μL) is taken and diluted with acetone (~2 mL) to serve as the initial concentration data point. The required amount of catalyst is then added to the RB to achieve an epoxide:Sn of 250:1. After adding the catalyst, the RB is immersed in a silicone oil bath, pre-heated to the desired temperature of 60 °C. This process introduces a brief non-isothermal step into the process that has a negligible effect on the calculated conversion since the steady state temperature is reached in less than two minutes. At specific times, a sample (40 μL) is withdrawn from the reaction mixture using a reusable stainless-steel needle and is filtered using a small plug of silica and diluted with acetone. The samples are analyzed using gas chromatography (Agilent, 7820A) equipped with flame ionization detector (GC-FID) and the conversion is computed using the internal standard method. Product identification is done using GC–MS (equipped with Agilent HP-5 ms Ultra Inert column) in positive ion mode (electron ionization).

2.6. Catalytic material reuse

The recycle experiment to test the reusability of catalyst is performed using the same catalytic testing procedure described above with the exception that the reaction is scaled up by a factor of four to facilitate recovering of catalyst for subsequent tests and the test is performed using a 25 mL RB. For each test, the amount of the reaction mixture is scaled to achieve a ratio of epoxide:Sn of 250:1 (0.4 mol% Sn). After each test, the catalyst is separated from the reaction mixture by centrifuging at 8500 RPM for 15 min. The separated catalyst is further washed using the same alcohol used in reaction (five times the volume of reaction mixture) and then dried at 90 °C overnight before using it for a subsequent cycle.

3. Result and discussion

3.1. Synthesis and material characterization

Initial work demonstrates the successful synthesis of nano-Beta zeolites at a Si:Sn ratio of 100:1 and 200:1. The materials are characterized using PXRD, demonstrating the successful formation of zeolite Beta. Compared to the typical hydrothermal synthesis, the PXRD peaks for nSnBeta are broader than Sn-Beta, consistent with the idea that small particles are present for nSnBeta. It should be mentioned that the Sn incorporation lengthens the crystallization time as compared to pure Si-Beta synthesized using the same procedure. The crystallization time is determined to be ~15 days for nSnBeta-200 and > 45 days for nSnBeta-100. While crystallization time increased, SEM analysis of nSnBeta materials reveals that the slower crystallization did not result in a significant increase in particle size for these materials, as shown in Fig. 1. The particle size and textural properties of all the materials synthesized are reported in Table 1. The nSnBeta materials exhibit higher external surface areas as compared to conventional Sn-Beta (cSnBeta-200). This difference is as expected given the smaller particle size of nSnBeta. The micropore volume is similar for these materials and is comparable to that of conventionally synthesized Sn-Beta. For the nSnBeta materials, the nitrogen physisorption isotherms have a hysteresis that can be attributed to interparticle pores that are common in the synthesis of nanomaterials as shown in Figure S1. The synthesis also

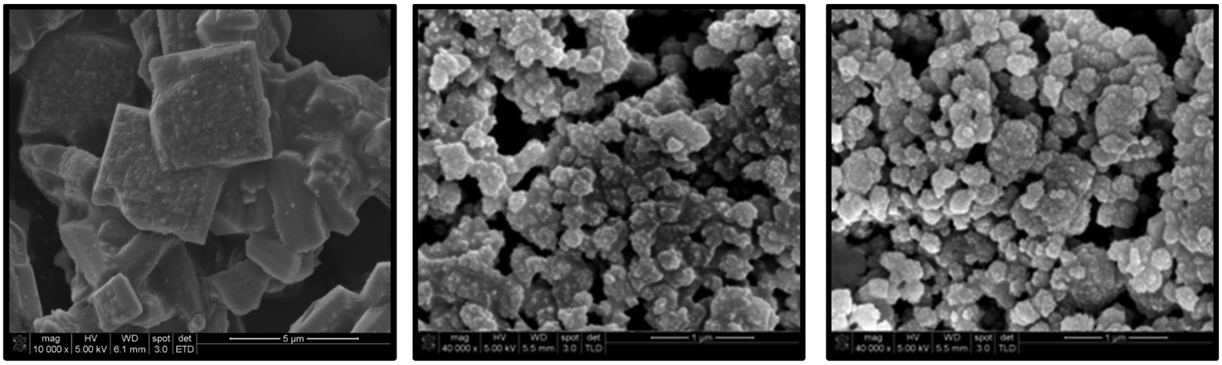

Fig. 1. SEM images of cSnBeta-100 (left), nSnBeta-100 (center), and nSnBeta-200 (right). The cSnBeta image is collected at 5 μm scale and nSnBeta images are 1 μm scale.

affects the morphology in addition to the particle size. For nSnBeta, SEM images provide visual indication that the material consists of berry-like clusters with an overall size of the cluster of ˜150 nm. The primary particle size is estimated from the pXRD data using the Scherrer equation (correcting for instrument broadening) to be approximately 20–40 nm. From SEM analysis, the conventional Sn-Beta is found to have a truncated bipyramidal morphology with a particle size of 1–5 μm, consistent with previous work.

The materials are further characterized using elemental analysis, DRUVS, and DRIFTS to investigate the incorporation of Sn into nSnBeta. Previously, nano SnMFI zeolite synthesis resulted in low Sn incorporation efficiency [17]. Interestingly, the synthesis conditions used for nSnBeta does not affect the Sn incorporation efficiency. The actual Si:Sn ratio for nSnBeta100 and nSnBeta200 is computed as 118 and 170, respectively. This is comparable to conventional Sn-Beta synthesis (Table 1). Understanding the differences in Sn incorporation for different zeolites represents an important challenge, but it is outside the scope of the present work.

DRIFTS and DRUVS analysis are performed to investigate the presence of framework Sn species. These techniques have been used previously to confirm the presence of framework Sn species [17,46–48]. DRUVS analysis can be used to identify presence of tin oxide (SnO_2), as it has a specific signature resulting in a peak at 280 nm. This peak is absent in the nSnBeta200, however for nSnBeta100 a low intensity broad peak is observed at 280 nm indicating that higher Sn incorporation can result in formation of SnO_2, as shown in Figure S2.

DRIFTS analysis with CD_3CN as the probe molecule is performed to obtain information about the types of Sn sites present in the material [47,49]. Conventionally, Sn-Beta is reported to have two types of Sn sites, open and closed that result in adsorbed CD_3CN having a distinct shift in the IR peak for the C—N bond. For nSnBeta, the DRIFTS spectrum consists of a large peak corresponding to silanols along with a small peak corresponding to framework Sn species (Figure S3). The DRIFTS spectra can be deconvoluted assuming both open and closed sites are present. Through deconvoluting the DRIFTS data, the ratio of open to closed sites is determined, as shown in Table 1. cSnBeta (Figure S4) is found to have the expected open:closed of 0.5:1, but the nSnBeta-100 and nSnBeta-200 have ratios of 1:1 and 1.5:1, respectively. Ongoing work is examining the differences in the open to closed site ratio for the epoxide ring opening reaction. The large silanol peak however indicates the higher density of silanols on these materials compared to cSnBeta, making the nSnBeta less hydrophobic as compared to the fluoride mediated synthesis of cSnBeta. This is also corroborated by a larger mass loss corresponding to physisorbed water on the TG curve for nSnBeta depicted in Figure S5. For nSnMFI, the DRIFTS spectrum consists of two peaks that can be attributed to acetonitrile adsorption on silanols and closed Sn sites (Figure S6). Overall, the results from DRIFTS and DRUVS analysis confirm that Sn is successfully incorporated in the framework of nSnBeta.

3.2. *Catalytic testing*

Initial catalytic testing examined the ring-opening reaction of epichlorohydrin with methanol. These substrates and the resultant products are relatively small, making it possible to compare catalytic performance of materials with minimal impact of internal or external mass transfer. Indeed, our previous work has demonstrated that these substrates react similarly when using the tin-substituted small pore zeolite Sn-MFI [17]. Analysis of catalytic behavior for materials with three different particle sizes of 80, 200, and 500 nm demonstrate that internal mass transfer limitations are minimal for these reactants. The catalytic testing of nSnBeta-200 and cSnBeta-200 shows that both catalysts result in complete conversion of epichlorohydrin in 24 h, as shown in Fig. 2. These catalysts result in similar regioselectivity for the terminal ether of 96%, consistent with our previous work [17,43]. The initial turnover frequency (TOF_0) of moles epoxides converted per mole Sn per hour is calculated for all of the materials. Both cSnBeta-200 and nSnBeta-200 have similar TOF_0 of 193 (moles epoxide per mole Sn per

Table 1
Summary of characterization of catalysts, including textural properties and composition.

Sample	Surface area[a] (m^2/g)	Micropore volume[b] (cm^3/g)	Theoretical Si/Sn	Actual Si/Sn[c]	Open:Closed Sites
nSnBeta-100	806	0.22	100	116	1:1
nSnBeta-200	740	0.23	200	170	1.5:1
cSnBeta-100	480	0.20	100	111	0.5:1
cSnBeta-200	468	0.20	200	237	0.5:1
nSnMFI-100	594	0.14	50	118	0:1
nSnBeta-200 Regenerated[d]	670	0.21	200	172	–

[a] Calculated using BET method for nitrogen physisorption data.
[b] Calculated using t-plot method for nitrogen physisorption data.
[c] Data obtained from ICP-OES analysis.
[d] Material is tested in three catalytic cycles before calcining to remove accumulated organic species.

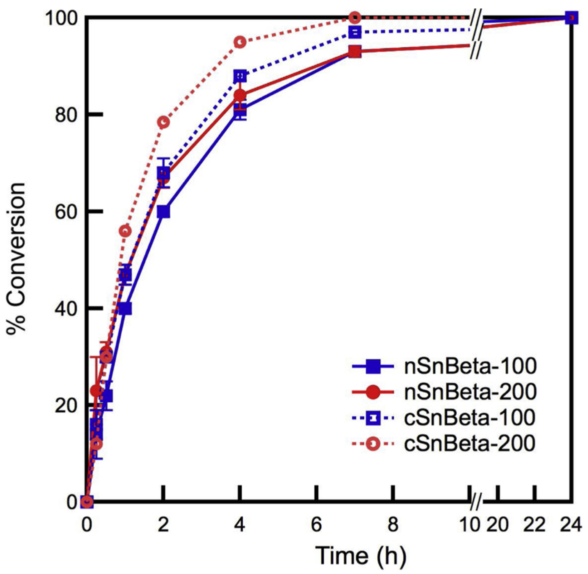

Fig. 2. Comparison of conversion of epichlorohydrin with methanol using nSnBeta-100, nSnBeta-200, cSnBeta-100, and cSnBeta-200. The amount of catalyst added is scaled to achieve an epoxide:Sn of 250:1. The reaction conditions are: 0.4 M epichlorohydrin in 2 mL methanol, 10 µL DGDE (internal standard), 60 °C, and 600 RPM.

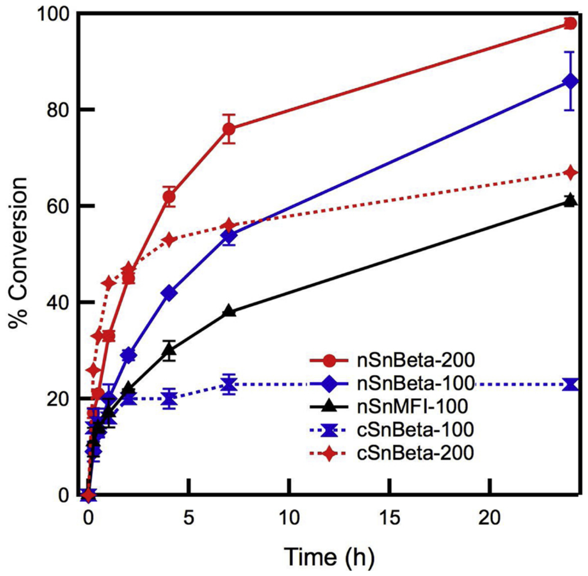

Fig. 3. Comparison of conversion of 1,2-epoxyocatane with ethanol using nSnBeta-100, nSnBeta-200, nSnMFI-100, cSnBeta-100, and cSnBeta-200. The amount of catalyst added is scaled to achieve an epoxide:Sn of 250:1. The reaction conditions are: 0.4 M 1,2-epoxyoctane in 2 mL ethanol, 50 µL DGDE (internal standard), 60 °C, and 600 RPM.

hour; cSnBeta-200) and 168 (nSnBeta-200). In comparison, nSnBeta-100 has a lower TOF_0 value of 129 than nSnBeta-200 and cSnBeta. This difference can be attributed to the presence of SnO_2 in nSnBeta-100, which is observed using DRUVS and has previously been demonstrated to have limited catalytic activity. The formation of SnO_2 appears to be an issue for the high loadings of Sn. Indeed, lower catalytic activity is also observed for the conventional cSnBeta-100 materials where the TOF_0 of 165 is calculated, which is lower than the TOF_0 found for cSnBeta-200.

After establishing the similarity of the different zeolites for small substrates, the effect of particle size on catalytic performance is tested by comparing the nano and conventional Sn-Beta materials for ring opening of 1,2-epoxyoctane with ethanol. For this reaction, the conversion over time is examined using cSnBeta-100 as a catalyst, as shown in Fig. 3. Initially, cSnBeta-100 is able to convert the epoxide with a high rate (initial turnover frequencies are reported in Table S1), but the apparent catalytic activity decreases after a conversion of 20%. The plateauing is associated with the pore filling as the longer diffusion length makes it difficult for the products to diffuse out of the catalyst. This is confirmed by analyzing the catalyst post-reaction using TGA-DSC (Figure S7). A mass loss of ~15% is observed between 200–700 °C, consistent with presence of organic content in the pores.

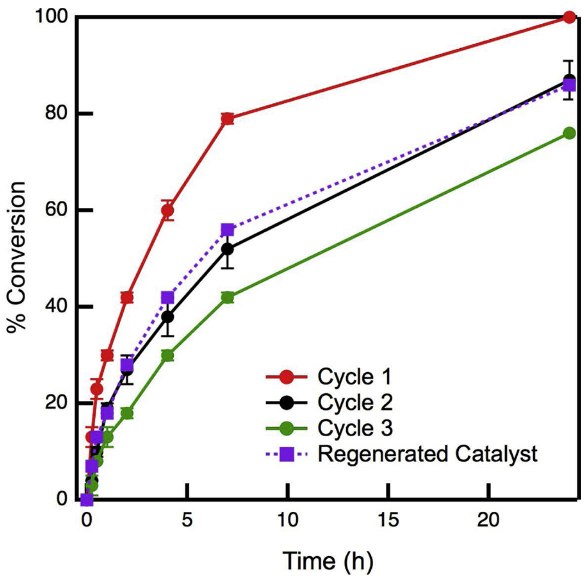

Fig. 4. Comparison of the conversion of 1,2-epoxyoctane over time (reacted with ethanol) for nSnBeta-200 for catalyst reusability testing. Fresh catalyst is used for cycle 1 that is recovered *via* centrifugation and used in a second catalytic cycle. After cycle 3, the catalyst is regenerated through calcination before testing again (dashed line). The amount of catalyst added is scaled to achieve an epoxide:Sn of 250:1. The reaction conditions are: 0.4 M 1,2-epoxyoctane in ethanol with DGDE (internal standard) using a temperature of 60 °C and a stir rate of 600 RPM.

This catalytic behavior is similar to conversion-over-time behavior observed previously for the ring-opening of 1,2-epoxyhexane with methanol using SnMFI [17]. Since synthesizing nano MFI zeolites overcame diffusion limitations for 1,2-epoxyhexane and methanol, nano MFI (nSnMFI-100) is tested for catalytic activity for 1,2-epoxyoctane and ethanol. As shown in Fig. 3 nSnMFI-100 initially converts the epoxide rapidly, but the rate of conversion slows down over time, reaching only 60% with a selectivity of 51% for terminal ether in 24 h. This suggests that the 10MR of MFI are limiting the overall catalytic performance.

The observed performance can be improved through examining a catalytic material with the pore size of zeolite Beta and a small particle size. Interestingly, nSnBeta-200 shows a significant improvement in catalytic performance reaching > 99% conversion of 1,2-epoxyoctane in 24 h with 57% selectivity for terminal ether, as shown in Fig. 3. This demonstrates the benefit of nano-zeolites with more open frameworks for bulkier substrates. When nSnBeta-100 is tested for the same substrates, it shows slightly lower catalytic activity as compared to nSnBeta-200. This difference can be attributed to the presence of SnO_2 species in nSnBeta-100, as SnO_2 has limited catalytic activity for this reaction [43].

With the reduction in particle size, it becomes important to determine if the improvement in catalytic activity is associated with reducing the particle size or if the synthesis results in catalytic sites on the external surface of the material. To test this, nSnBeta-100 and nSnBeta-200 are tested for ring opening of 1,2-epoxycyclododecane with

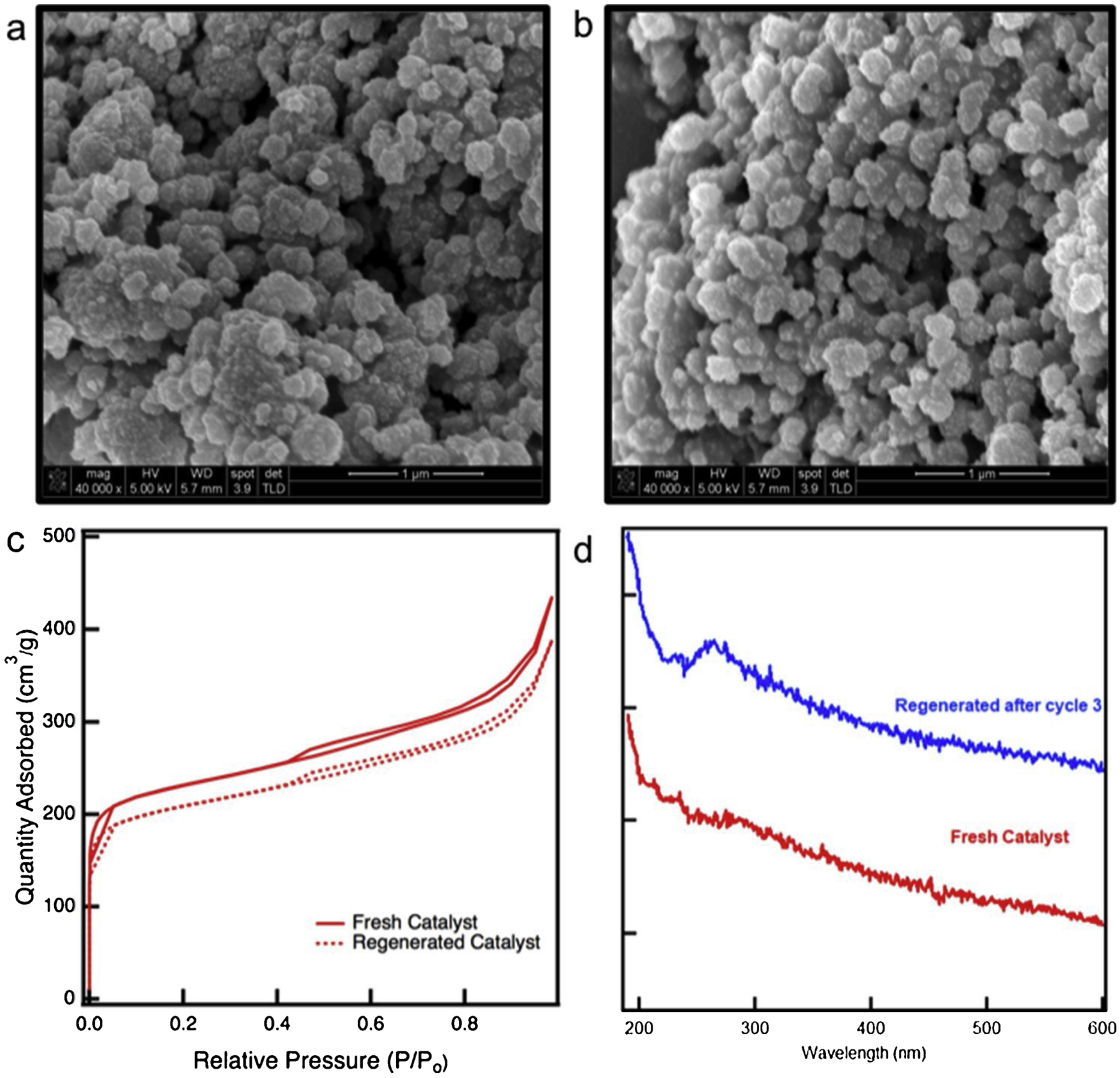

Fig. 5. Characterization of fresh nSnBeta-200 catalyst compared to the regenerated catalyst after recycle experiment. (a) SEM images at 1 μm magnification of fresh nSnBeta-200 and (b) regenerated nSnBeta-200. (c) Nitrogen physisorption isotherms for the fresh and regenerated nSnBeta-200 as well as (d) the DRUV spectra for the fresh and regenerated nSnBeta-200.

methanol. This substrate is selected considering that it is too bulky to enter the pores of zeolite beta. Therefore, the observed catalytic activity would be associated with the surface sites. Both nSnBeta and cSnBeta catalysts result in similar conversion of 5% (cSnBeta) and 8% (nSnBeta) conversion of 1,2-epoxycyclododecane in 24 h. The slight difference in conversion could reflect that nSnBeta has a greater external surface area than cSnBeta, but the difference is generally considered to be within the margin of error for these measurements. This appears to be associated with catalytic sites on surface since a similar reaction in the absence of catalyst results in no conversion of the bulky epoxide. This indicates that nSnBeta and cSnBeta have similar amounts of catalytic sites on the external surface and that the majority of the active sites are within the pores of zeolites and not on the surface.

3.3. *Catalyst reuse testing*

These results are promising provided that the catalyst can be reused. Using 1,2-epoxyoctane and ethanol as substrates, the conversion *versus* time data for the first cycle is similar to the small-scale tests performed, as shown in Fig. 4. However, it is observed that activity as well as final conversion reduces for subsequent cycles. The reduction in catalytic activity could be attributed to pore filling and/or leaching of Sn from the framework. The catalyst recovered after third cycle is analyzed using TGA-DSC and results are shown in Figure S8. A mass loss of ~10% is observed between 200–500 °C confirming accumulation of organic content in the pores of the catalyst. This is consistent with the organic content observed after one catalytic cycle (Figure S9). To test if the activity can be recovered, the organic content is removed by calcining the catalyst at 550 °C. In addition, the Sn content in the reused catalyst is analyzed using ICP-OES giving a Si:Sn ratio of 172 as compared to 170 for the fresh catalyst. This result confirms that leaching is not the main cause of deactivation. The recovered calcined catalyst is tested for ring opening of 1,2-epoxyoctane with ethanol and the amount of catalyst is adjusted to keep epoxide: Sn ratio of 250:1. The catalytic activity for regenerated catalyst is lower compared to the fresh catalyst. This can be caused either by loss of crystallinity, increase in particle size because of aggregation, or increase in the amount of SnO_2. To understand the cause of decreased catalytic activity, the calcined catalyst after the third cycle of recyclability test is analyzed using PXRD, nitrogen physisorption, SEM, and DRUVS. The results show that the materials remain crystalline and the particle size remains constant, as shown in Figure S10 and Fig. 5, respectively. From nitrogen physisorption, it is determined that the surface area decreases by approximately 10% relative to the fresh catalyst (Table 1). While this is a measurable decrease, it is less than the decrease in initial TOF. The initial decrease in TOF from 99 to 54 per hour appears to be correlated with an increase in the formation of SnO_2 in the recycled catalyst, as shown in Fig. 5. While the fresh catalyst does not have a peak in the DRUV spectrum at 280 nm that would be consistent with SnO_2, the DRUV spectrum for the catalyst recovered from one reaction cycle is determined to have a peak at 280 nm that could be consistent with SnO_2 formation. Since our previous work indicates that SnO_2 has limited catalytic activity [43], the observed decrease in catalytic performance is likely associated with SnO_2 formation. In comparison, cSnBeta has previously been demonstrated to retain high catalytic activity over multiple catalytic cycles [43]. This difference in catalyst reusability between nSnBeta and cSnBeta suggests that the low defect framework produced in hydrothermal conditions in the presence of fluoride is more stable than the framework produced in hydrothermal conditions in the presence of hydroxide. Despite the initial decrease in activity, nSnBeta is able to retain moderate catalytic activity upon calcination and achieve high conversion. Overall, the catalytic activity at high conversion of nSnBeta appears higher than the cSnBeta, demonstrating the merit of synthesizing Lewis acidic nanozeolites.

4. Summary

Lewis acidic nSnBeta zeolites are synthesized by using a low temperature synthesis with $TMP(OH)_2$ as the SDA. It is demonstrated that the final particle size of nSnBeta is not influenced by the amount of Sn incorporated into the material since a particle size of ~150 nm is observed for both nSnBeta-100 and nSnBeta-200. The catalytic testing of nSnBeta using epichlorohydrin ring opening with methanol shows that nSnBeta material are active catalysts for epoxide ring opening reaction. The real advantage of particle size reduction is observed for ring opening of bulky 1,2-epoxyoctane with ethanol where enhanced catalytic activity is observed for nSnBeta as compared to cSnBeta materials. Catalytic testing with 1,2-epoxycyclododecane with methanol demonstrates that the catalytic sites are located inside the pores of the zeolite. The nano zeolite (nSnBeta) can be used in multiple catalytic cycles with a moderate loss in catalytic activity after each cycle. The catalytic performance of nSnBeta especially at high conversions is higher than cSnBeta even for the reused catalyst. The catalytic activity of the used catalyst can be significantly recovered by regeneration with calcination. Overall, nSnBeta is a highly active catalyst for the epoxide ring opening reaction involving bulky substrates.

Competing interest

The authors declare no competing interest.

Acknowledgements

We gratefully acknowledge the American Chemical Society Petroleum Research Fund (ACS-PRF 55946-DNI5), the National Science Foundation (NSF Career 1653587), and the Ohio State University Institute for Materials Research (OSU IMR FG0211 and EMR-G00018) for their financial support.

Appendix A. Supplementary data

Supplementary material related to this article can be found, in the online version, at doi:https://doi.org/10.1016/j.apcata.2019.03.009.

References

[1] P. Wolf, C. Hammond, S. Conrad, I. Hermans, Dalton Trans. 43 (2014) 4514.
[2] Y. Wang, J.D. Lewis, Y. Roman-Leshkov, ACS Catal. 6 (2016) 2739.
[3] A. Corma, M. Renz, M. Boronat, P. Concepcio, Catal. Today 121 (2007) 39.
[4] T. Blasco, M.A. Camblor, A. Corma, P. Esteve, J.M. Guil, A. Martínez, J.A. Perdigón-Melón, S. Valencia, A. Martinez, J. Perdigon-Melon, S. Valencia, J. Phys. Chem. B 102 (1998) 75.
[5] R. Bermejo-Deval, M. Orazov, R. Gounder, S.-J. Hwang, M.E. Davis, ACS Catal. 4 (2014) 2288.
[6] R. Bermejo-Deval, R. Gounder, M.E. Davis, ACS Catal. 2 (2012) 2705.
[7] M. Moliner, Y. Roman-Leshkov, M.E. Davis, Proc. Natl. Acad. Sci. 107 (2010) 6164.
[8] A. Corma, M.E. Domine, L. Nemeth, S. Valencia, J. Am. Chem. Soc. 124 (2002) 3194.
[9] J. Dijkmans, W. Schutyser, M. Dusselier, B.F. Sels, Chem. Commun. 52 (2016) 6712.
[10] A. Corma, L.T. Nemeth, M. Renz, S. Valencia, Nature 1433 (2001) 423.
[11] M. Boronat, P. Concepción, A. Corma, M. Renz, S. Valencia, J. Catal. 234 (2005) 111.
[12] J.J. Pacheco, M.E. Davis, Proc. Natl. Acad. Sci. U.S.A. 111 (2014) 8363.
[13] J.D. Lewis, S. Van De Vyver, R. Rodríguez, S. Van de Vyver, Y. Roman-Leshkov, Angew. Chemie Int. Ed. 54 (2015) 9835.
[14] M. Su, W. Li, T. Zhang, H.S. Xin, S. Li, W. Fan, L. Ma, Catal. Sci. Technol. 7 (2017) 3555.
[15] S. Hwang, W.S. Chi, S.J. Lee, S.H. Im, J.H. Kim, J. Kim, J. Memb. Sci. 480 (2015) 11.
[16] B. Tang, W. Dai, G. Wu, N. Guan, L. Li, M. Hunger, ACS Catal. 4 (2014) 2801.
[17] A. Parulkar, R. Joshi, N. Deshpande, N.A. Brunelli, Appl. Catal. A Gen. 566 (2018) 25.
[18] K. Zhang, M.L. Ostraat, Catal. Today 264 (2016) 3.
[19] J. Pérez-Ramírez, C.H. Christensen, K. Egeblad, C.H. Christensen, J.C. Groen, Chem. Soc. Rev. 37 (2008) 2530.
[20] D. Verboekend, J. Pérez-Ramírez, Catal. Sci. Technol. 1 (2011) 879.
[21] O. Larlus, S. Mintova, S.T. Wilson, R.R. Willis, H. Abrevaya, T. Bein, Microporous Mesoporous Mater. 142 (2011) 17.
[22] X. Yang, Y. Liu, X. Li, J. Ren, L. Zhou, T. Lu, Y. Su, ACS Sustain. Chem. Eng. 6 (2018) 8256.
[23] B. Modhera, M. Chakraborty, P.A. Parikh, R.V. Jasra, Cryst. Res. Technol. 44 (2009) 379.
[24] M.S. Holm, E. Taarning, K. Egeblad, C.H. Christensen, Catal. Today 168 (2011) 3.
[25] M. Choi, K. Na, J.Y. Kim, Y. Sakamoto, O. Terasaki, R. Ryoo, Nature 461 (2009) 246.
[26] J. Kim, J. Chun, R. Ryoo, Chem. Commun. 51 (2015) 13102.
[27] M.A. Camblor, A. Mifsud, J. Pérez-Pariente, Zeolites 11 (1991) 792.
[28] M.A. Camblor, J. Pérez-Pariente, Zeolites 11 (1991) 202.
[29] O. Larlus, V. Valtchev, Microporous Mesoporous Mater. 93 (2006) 55.
[30] Y. Kalvachev, T. Todorova, L. Dimitrov, V. Valtchev, Microporous Mesoporous Mater. 177 (2013) 11.
[31] I. Schmidt, C. Madsen, C.J.H. Jacobsen, Inorg. Chem. 39 (2000) 2279.
[32] Z. Zhu, H. Xu, J. Jiang, H. Wu, P. Wu, ACS Appl. Mater. Interfaces 9 (2017) 27273.
[33] R. Martínez-Franco, C. Paris, M.E. Martínez-Armero, C. Martínez, M. Moliner, A. Corma, Chem. Sci. 7 (2016) 102.
[34] X. Cheng, J. Mao, X. Lv, T. Hua, X. Cheng, Y. Long, Y. Tang, J. Mater. Chem. A 2 (2014) 1247.
[35] M.M. Reddy, M.A. Kumar, P. Swamy, M. Naresh, K. Srujana, L. Satyanarayana, A. Venugopal, N. Narender, Green Chem. 15 (2013) 3474.
[36] S. Tolborg, A. Katerinopoulou, D.D. Falcone, I. Sadaba, C.M. Osmundsen, R.J. Davis, E. Taarning, P. Fristrup, M.S. Holm, J. Mater. Chem. A 2 (2014) 20252.
[37] S. Valencia, A. Corma, Stannosilicate Molecular Sieves (1999).
[38] P. Li, G. Liu, H. Wu, Y. Liu, J.G. Jiang, P. Wu, J. Phys. Chem. C 115 (2011) 3663.
[39] H. Xu, X. Wang, P. Ji, H. Wu, Y. Guan, P. Wu, Inorg. Chem. Front. 5 (2018) 2763.
[40] C. Hammond, S. Conrad, I. Hermans, Angew. Chem. Int. Ed. 51 (2012) 11736.
[41] H. Robson, J. Garces, H. Kessler, A.N. Kotasthane, H. Lechert, B. Schoeman, S. Wilson, Verified Syntheses of Zeolitic Materials (2001).
[42] B. Tang, W. Dai, X. Sun, G. Wu, N. Guan, M. Hunger, L. Li, Green Chem. 17 (2015) 1744.
[43] N. Deshpande, A. Parulkar, R. Joshi, B. Diep, A.R. Kulkarni, N.A. Brunelli, J. Catal. 370 (2019) 46.
[44] W. Dai, C. Wang, B. Tang, G. Wu, N. Guan, Z. Xie, M. Hunger, L. Li, ACS Catal. 6 (2016) 2955.
[45] G. Prestat, C. Baylon, M.P. Heck, C. Mioskowski, Tetrahedron Lett. 41 (2000) 3829.
[46] S. Roy, K. Bakhmutsky, E. Mahmoud, R.F. Lobo, R.J. Gorte, ACS Catal. 3 (2013) 573.
[47] V.L. Sushkevich, I.I. Ivanova, A.V. Yakimov, J. Phys. Chem. C 121 (2017) 11437.
[48] J.W. Harris, M.J. Cordon, J.R. Di Iorio, J.C. Vega-Vila, F.H. Ribeiro, R. Gounder, J. Catal. 335 (2016) 141.
[49] W.R. Gunther, V.K. Michaelis, R.G. Griffin, Y. Roman-Leshkov, J. Phys. Chem. C 120 (2016) 28533.